Review

Magnetic Resonance in Chemistry

Received: 20 April 2010 Revised: 2 June 2010 Accepted: 4 June 2010 Published online in Wiley Online Library: 12 July 2010

(wileyonlinelibrary.com) DOI 10.1002/mrc.2646

Prediction of NMR *J*-coupling in solids with the planewave pseudopotential approach†

Jonathan R. Yates*

We review the calculation of NMR *J*-coupling in solid materials using the planewave pseudopotential formalism of Density Functional Theory. The methodology is briefly summarised and an account of recent applications is given. We discuss various aspects of the calculations which should be taken into account when comparing results with solid-state NMR experiments including anisotropy and orientation of the *J* tensors, the reduced coupling constant, and the relation between *J* and crystal structure.

Keywords: solid-state NMR; *J*-coupling; DFT; planewave pseudopotential; GIPAW

Introduction

Together with the chemical shielding and electric field gradient the *J*-coupling is a key quantity in solid-state NMR experiments, providing information on the local atomic environment in a material. *J*-coupling is often utilised in multi-dimensional NMR experiments but there are relatively few reports of measured values of *J* in solids – as compared to the chemical shift or Electric Field Gradient (EFG). This is particularly true for lighter elements and for two bond and more distant coupling, as in such cases *J* is often sufficiently small as to be hidden by the line width. However, advances in experimental technique such as accurate setting of the magic angle, very high spinning speeds together with the availability of high-field spectrometers have stimulated interest in measuring small *J*-couplings (see Ref. [1] for a recent summary). Highlights have included the observation of two *J*-couplings between a given spin pair,[2] the measurement of distributions of *J* in amorphous materials,[3] and reports of *J* as low as 1.5 Hz.[4]

First principles quantum mechanical calculations have an important role to play in the interpretation of NMR experiments on complex materials. The Linear Augmented Planewave (LAPW) approach in its implementation within the Wien series of codes[5] has been widely used and shown to reliably predict EFG tensors.[6] In the past decade the Gauge Including Projector Augmented Wave (GIPAW) approach[7] has been used to compute chemical shielding (CSA) tensors and EFGs within the planewave pseudopotential formalism of density functional theory. More recent work has enabled *J* tensors in solids to be computed within this framework.[8] Only a few initial applications of this approach have been published.[8–11] However, we take this early opportunity to highlight some issues which should be considered when making the comparison both with experiments and with quantum chemical approaches applied to cluster models of solids. Comprehensive reviews exist for many related topics including calculation of *J* tensors using quantum chemical approaches,[12–14] calculations of chemical shifts and electric field gradients in solids[15,16] and introductions to first principles materials modelling.[17,18]

Theory

In an effective nuclear spin Hamiltonian, we can identify spin–spin coupling with a term of the form

$$H = \sum_{K<L} \mathbf{I}_K (\mathbf{D}_{KL} + \boldsymbol{J}_{KL}) \mathbf{I}_L \tag{1}$$

Here the nucleus K has spin angular momentum $\hbar\mathbf{I}_K$ and an associated magnetic moment $\boldsymbol{\mu}_K = \gamma_K \hbar \mathbf{I}_K$ where γ_K is a nuclear constant known as the magnetogyric ratio. $\mathbf{D}_{KL}$ is the direct dipolar coupling between the two nuclei and is a function of the nuclear constants and the internuclear distance. $\boldsymbol{J}_{KL}$ is the indirect coupling and represents an interaction mediated by the bonding electrons. The *J*-coupling is a small perturbation to the electronic ground-state of the system, and we can identify it as a derivative of the total electronic energy *E*, of the system

$$\boldsymbol{J}_{KL} = \frac{\hbar \gamma_K \gamma_L}{2\pi} \frac{\partial^2 E}{\partial \boldsymbol{\mu}_K \partial \boldsymbol{\mu}_L} \tag{2}$$

An equivalent expression arises from considering one nuclear spin (L) as perturbation which creates a magnetic field at a second (receiving) nucleus (K)

$$\mathbf{B}_{in}^{(1)}(\mathbf{R}_K) = \frac{2\pi}{\hbar \gamma_K \gamma_L} \boldsymbol{J}_{KL} \cdot \boldsymbol{\mu}_L \tag{3}$$

Equation (3) tells us that the question of computing *J* is essentially that of computing the magnetic field induced indirectly by a nuclear magnetic moment. The first complete analysis of this

* *Correspondence to: Jonathan R. Yates, Department of Materials, University of Oxford, Oxford OX1 3PH, UK. E-mail: jonathan.yates@materials.ox.ac.uk*

† *Paper published as part of the Quantum-Chemical Calculations and their applications special issue.*

Department of Materials, University of Oxford, Oxford OX1 3PH, UK

indirect coupling was provided by Ramsey.[19,20] When spin–orbit coupling is neglected, we can consider the field as arising from two, essentially independent, mechanisms. Firstly, the magnetic moment can interact with electronic charge inducing an orbital current – which in turn creates a magnetic field at the other nuclei in the system. This mechanism is similar to the case of magnetic shielding in insulators which arises from the orbital currents induced by a uniform external field. The second mechanism arises from the interaction of the magnetic moment with the electronic spin, causing an electronic spin polarisation (i.e. the 'up' and 'down' spin charge densities are no longer identical). The resulting spin density creates a magnetic field through a hyperfine interaction. This is similar to the case of the Knight shift in a metallic system. To examine these contributions in more detail, we decompose the electronic Hamiltonian for the two coupled nuclei as:

$$\mathrm{H} = \frac{1}{2}\mathbf{p}^2 + \mathrm{V}(\mathbf{r}) + \mathrm{H}_{\mathrm{DSO}} + \mathrm{H}_{\mathrm{PSO}} + \mathrm{H}_{\mathrm{FC}} + \mathrm{H}_{\mathrm{SD}} \tag{4}$$

Here $V(\mathbf{r})$ is the all-electron local potential (including terms such as the Coulomb potential from the nuclei and the Hartree potential) and the other terms are as follows; the diamagnetic spin orbit (DSO),

$$\mathrm{H}_{\mathrm{DSO}} = \left(\frac{\mu_0}{4\pi}\right)^2 \frac{(\boldsymbol{\mu}_{\mathrm{L}} \times \mathbf{r}_{\mathrm{L}})}{|\mathbf{r}_{\mathrm{L}}|^3} \cdot \frac{(\boldsymbol{\mu}_{\mathrm{K}} \times \mathbf{r}_{\mathrm{K}})}{|\mathbf{r}_{\mathrm{K}}|^3} \tag{5}$$

the paramagnetic spin orbit (PSO),

$$\mathrm{H}_{\mathrm{PSO}} = \frac{\mu_0}{4\pi}\boldsymbol{\mu}_{\mathrm{B}} \cdot \frac{(\mathbf{r}_{\mathrm{L}} \times \mathbf{p})}{|\mathbf{r}_{\mathrm{L}}|^3} \tag{6}$$

the Fermi-contact (FC),

$$\mathrm{H}_{\mathrm{FC}} = g\beta\frac{\mu_0}{4\pi}\frac{8\pi}{3}\mathbf{S} \cdot \boldsymbol{\mu}_{\mathrm{L}}\,\delta(\mathbf{r}_{\mathrm{L}}) \tag{7}$$

and the spin–dipolar (SD),

$$\mathrm{H}_{\mathrm{SD}} = g\beta\frac{\mu_0}{4\pi}\mathbf{S} \cdot \left(\frac{3\mathbf{r}_{\mathrm{L}}(\boldsymbol{\mu}_{\mathrm{L}} \cdot \mathbf{r}_{\mathrm{L}}) - r_{\mathrm{L}}^2\boldsymbol{\mu}_{\mathrm{L}}\mathbf{1}}{|r_{\mathrm{L}}|^5}\right) \tag{8}$$

Here $\mathbf{r}_{\mathrm{L}} = \mathbf{r} - \mathbf{R}_{\mathrm{L}}$ with $\mathbf{R}_{\mathrm{L}}$ the position of nucleus L, μ_0 is the permeability of a vacuum, δ is the Dirac delta function, $\boldsymbol{S}$ is the Pauli spin operator, g the Landé g-factor and β is the Bohr magneton.

The FC and SD terms give rise to a spin magnetisation density $\boldsymbol{m}(\boldsymbol{r})$, and the DSO and PSO terms induce a current density, $\boldsymbol{j}(\boldsymbol{r})$. By working to first order in these quantities we can write the magnetic field at atom K induced by the magnetic moment of atom L as

$$\begin{aligned}\mathbf{B}_{\mathrm{in}}^{(1)}(\mathbf{R}_{\mathrm{K}}) = {} & \frac{\mu_0}{4\pi}\int \mathbf{m}^{(1)}(\mathbf{r}) \cdot \left[\frac{3\mathbf{r}_{\mathrm{K}}\mathbf{r}_{\mathrm{K}} - |\mathbf{r}_{\mathrm{K}}|^2}{|\mathbf{r}_{\mathrm{K}}|^5}\right] \mathrm{d}^3\mathbf{r} \\ & + \frac{\mu_0}{4\pi}\frac{8\pi}{3}\int \mathbf{m}^{(1)}(\mathbf{r})\delta(\mathbf{r}_{\mathrm{K}})\,\mathrm{d}^3\mathbf{r} \\ & + \frac{\mu_0}{4\pi}\int \mathbf{j}^{(1)}(\mathbf{r}) \times \frac{\mathbf{r}_{\mathrm{K}}}{|\mathbf{r}_{\mathrm{K}}|^3}\,\mathrm{d}^3\mathbf{r}.\end{aligned} \tag{9}$$

Formally $\boldsymbol{J}$ can be described by a 3×3 matrix, where the elements refer to the Cartesian components of the two spins. Physically this reflects the fact that for a given Cartesian orientation of the magnetic moment of the perturbing nucleus, say z, the magnetic field at the receiving nucleus will, in general, have components along each of x, y and z. $\boldsymbol{J}$ can be decomposed into symmetric $\boldsymbol{J}^{\mathrm{sym}}$, and antisymmetric $\boldsymbol{J}^{\mathrm{anti-sym}}$ contributions, i.e. $\boldsymbol{J}^{\mathrm{sym}} = (\boldsymbol{J} + \boldsymbol{J}^{\dagger})/2$ where $\boldsymbol{J}^{\dagger}$ represents the transpose of $\boldsymbol{J}$. As for the case of the magnetic shielding tensor, to first order only the symmetric part of $\boldsymbol{J}$ directly affects the observed NMR spectrum. The isotropic $\boldsymbol{J}$ coupling is given by the one third of trace of $\boldsymbol{J}$ and the anisotropy can be defined as

$$\Delta\boldsymbol{J} = \mathrm{J}_{zz} - \frac{1}{2}(\mathrm{J}_{xx} + \mathrm{J}_{yy}) \tag{10}$$

where J_{zz}, J_{yy} and J_{xx} are the principal components of $\boldsymbol{J}^{\mathrm{sym}}$, labelled according to $|\mathrm{J}_{yy} - \mathrm{J}_{\mathrm{iso}}| > |\mathrm{J}_{yy} - \mathrm{J}_{\mathrm{iso}}| > |\mathrm{J}_{yy} - \mathrm{J}_{\mathrm{iso}}|$

We can decompose $\mathbf{B}_{\mathrm{in}}^{(1)}(\mathbf{R}_{\mathrm{K}})$ and hence the total $\boldsymbol{J}$-coupling tensor into five components:

$$\boldsymbol{J} = \boldsymbol{J}^{\mathrm{DSO}} + \boldsymbol{J}^{\mathrm{PSO}} + \boldsymbol{J}^{\mathrm{FC}} + \boldsymbol{J}^{\mathrm{SD}} + \boldsymbol{J}^{\mathrm{SD/FC}} \tag{11}$$

The term $\boldsymbol{J}^{\mathrm{SD/FC}}$ arises from a magnetisation induced by a Fermi-contact mechanism at the perturbing site, which in term induces a magnetic field at the receiving site through a spin–dipolar mechanism. The remaining terms arise from the same coupling mechanism at the perturbing and receiving sites, e.g. $\boldsymbol{J}^{\mathrm{SD}}$ corresponds to magnetisation created by a spin–dipolar interaction, which then creates a magnetic field at the receiving nucleus by a spin–dipolar interaction. By considering the form of the operators in Eqns (5)–(8), we can identify if a term contributes to the isotropy, anisotropy or both aspects of the $\boldsymbol{J}$ tensor. For example, the FC operator gives a magnetic field which is parallel to the nuclear moment. As a result $\boldsymbol{J}^{\mathrm{FC}}$ is purely isotropic. By a similar argument $\boldsymbol{J}^{\mathrm{SD/FC}}$ contributes only to the anisotropic component of the tensor $\boldsymbol{J}$. The remaining terms contribute to both the isotropic and anisotropic part of $\boldsymbol{J}$.

Implementation

Periodic boundary conditions

In electronic structure simulations it is common practise to treat a crystalline material by considering the primitive unit cell under periodic boundary conditions. In this circumstance, an atom in the primitive cell would experience the same electronic environment as if it were in an infinite crystal. In order to compute the $\boldsymbol{J}$ coupling we consider the coupling between the perturbing nucleus and all other nuclear spins in the system. By making one atom different, we have broken the translational symmetry of the crystal. For small primitive cells, there will be an interaction between the perturbing atom and its periodic images, as illustrated in Fig. 1. Such a situation would also occur when modelling a defect site in a crystal. In this case, it is necessary to perform calculations on a supercell (multiple of the primitive cell), so that this spurious interaction has negligible effect. Fortunately, the interaction between magnetic dipoles converges rapidly and tests with supercells of increasing size on silicophosphate[8] and molecular crystals[9] found that ~10 Å between an atom and its nearest periodic image was sufficient to give converged results.

It can be seen from Eqns (5)–(8) that the operators responsible for $\boldsymbol{J}$-coupling are short ranged. This may cause us to question the need for a solid-state approach for the calculation of $\boldsymbol{J}$. However, the quantities the operators act on – wavefunctions and electronic charge density – are influenced by the long range electrostatics of the material. Quantifying these solid-state effects on $\boldsymbol{J}$ remains an

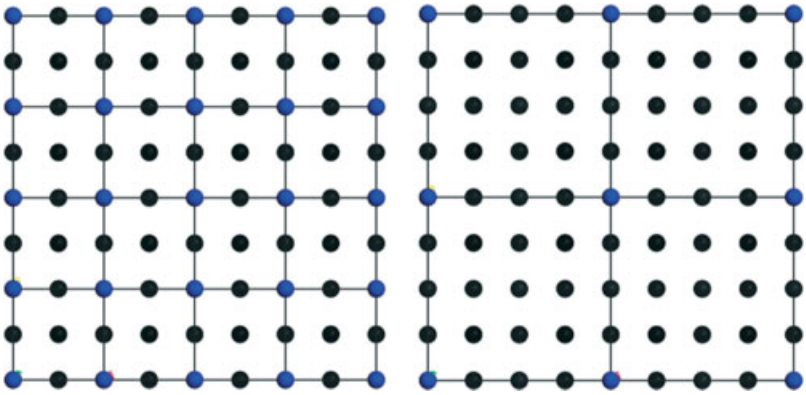

Figure 1. Representation of a supercell. Left: primative unit cell – perturbing site, and its periodic images are marked in blue. Right: 2 × 2 supercell of the primative cell.

open question. For the case of molecular crystals a study of Van der Waals bonded molecules[9] has shown that even when there are no strong intermolecular interactions solid-state effects on ***J*** couplings can be significant, and within the limits of experimental detection.

Planewaves, pseudopotentials and projector augmented wave method

In order to represent objects such as a charge density or a wavefunction, it is necessary to expand them in some form of basis set. For solid-state calculations a convenient choice is a set of planewaves. Essentially this means performing a Fourier expansion of quantity – so long as the waves are chosen to have a wavelength commensurate with the crystallographic unit cell they will automatically satisfy periodic boundary conditions. The size of the basis set is increased by including waves with successively shorter wavelengths (i.e. increasing kinetic energy). The quality of the basis set is conveniently specified by the maximum energy of the set of planewaves. A planewave basis has several advantages; including its simplicity, and the fact that it enables easy parallelism. One can distribute Fourier coefficients amongst nodes in a compute cluster – on systems with a good quality interconnect this can be efficient up to about a hundred nodes. However, an inherent complication in the use of planewaves is the requirement to describe the core–valence interaction through a pseudopotential. While this dramatically reduces the number of planewaves needed to obtain converged results, it does so at the cost of giving the valence wavefunctions an unphysical form close to the nucleus (as shown in panel (a) of Fig. 2). The combination of pseudopotentials and a planewave basis has proved to give a reliable description of many material properties, such as vibrational spectra and dielectric response,[21,22] but properties which depend critically on the wavefunction close to

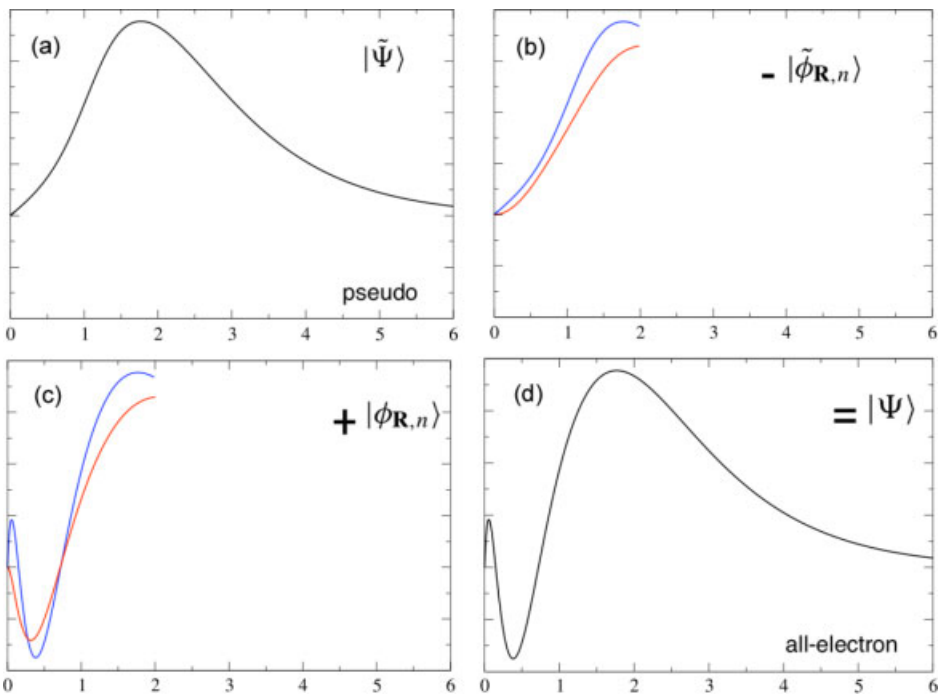

Figure 2. Schematic representation of the PAW transformation in Eqn (12). The *x*-axis represents radial distance from a nucleus. (a) Representation of the pseudowavefunction; (b) pseudo-atomic like states; (c) all-electron atomic-like states; (d) all-electron wavefunction.

the nucleus, such as NMR observables require careful treatment. The current standard approach to computing such properties is the projector augmented wave method (PAW) introduced by Blöchl[23] which provides a formalism to reconstruct the all-electron wavefunction from its pseudo counterpart, and hence obtain all-electron properties from calculations based on the use of pseudopotentials. This approach was adapted by Pickard and Mauri to give the GIPAW approach to compute magnetic shielding tensors,[7] however, to compute ***J*** the original PAW approach is sufficient. ***J***-coupling provides a tough test of the PAW formalism as we must perform a PAW reconstruction both at the perturbing site, in order to obtain the correct first order response (either an induced current, or magnetisation density), and again at the receiving site to obtain the induced magnetic field.

The PAW scheme proposes a linear transformation from the pseudowavefunction $|\tilde{\Psi}\rangle$, to the true all-electron wavefunction $|\Psi\rangle$, ie $|\Psi\rangle = \mathbf{T}|\tilde{\Psi}\rangle$, where

$$\mathbf{T} = \mathbf{1} + \sum_{\mathbf{R},n} [|\phi_{\mathbf{R},n}\rangle - |\tilde{\phi}_{\mathbf{R},n}\rangle]\langle\tilde{p}_{\mathbf{R},n}| \qquad (12)$$

$|\phi_{\mathbf{R},n}\rangle$ is a localised atomic state (say 3p) and $|\widetilde{\phi}_{\mathbf{R},n}\rangle$ is its pseudized counter part. $|\widetilde{p}_{\mathbf{R},n}\rangle$ are a set of functions which project out the atomic-like contributions from $|\tilde{\Psi}\rangle$. This equation is represented pictorially in Fig. 2. For an all-electron local or semi-local operator O, the corresponding pseudo-operator, $\widetilde{O}$, is given by

$$\widetilde{O} = O + \sum_{\mathbf{R},n,m} |\widetilde{p}_{\mathbf{R},n}\rangle[\langle\phi_{\mathbf{R},n}|O|\phi_{\mathbf{R},m}\rangle - \langle\widetilde{\phi}_{\mathbf{R},n}|O|\widetilde{\phi}_{\mathbf{R},m}\rangle]\langle\widetilde{p}_{\mathbf{R},m}| \qquad (13)$$

As constructed in Eqn (13) the pseudo-operator $\widetilde{O}$ acting on pseudo-wavefunctions will give the same matrix elements as the all-electron operator O acting on all-electron wavefunctions. Pseudo-operators for the ***J*** coupling operators given in Eqns (5)–(8) are reported in Ref. [8].

In contrast, most quantum chemical calculations employ a basis set of Gaussian type orbitals. Here convergence is reached by including more Gaussian type functions, for example with higher angular momentum coefficients. It has been observed[13,24] that the Fermi-contact operator is particularly difficult to describe as it samples the electronic wavefunction only at the nuclear position. Very large number of basis functions are needed to numerically converge this contribution. Jensen[24] has developed a series of Gaussian basis-sets optimised to provide a systematically improvable description of ***J***. In Fig. 3 we show the convergence with planewave energy of the Ramsey contributions to $^1\boldsymbol{J}_{CF}$ in CHF_3 within the PAW approach. It is clear from the graph that each term converges smoothly to the basis set limit: at 80 Ryd the FC term is within 0.2 Hz of its value at 140 Ryd, and the other terms are within 0.1 Hz of their limiting values.

In the planewave/PAW approach the Fermi-contact term presents no special difficulty. To understand this difference, we examine the form of the Fermi-contact operator in the PAW scheme

$$\widetilde{\mathrm{H}}_{\mathrm{FC}} = \mathrm{C} \sum_{n,m} |\widetilde{p}_{\mathbf{R}_\mathrm{L},n}\rangle\langle\phi_{\mathbf{R}_\mathrm{L},n}|\delta(\mathbf{r}_\mathrm{L})|\phi_{\mathbf{R}_\mathrm{L},m}\rangle\langle\widetilde{p}_{\mathbf{R}_\mathrm{L},m}| \qquad (14)$$

Where C represents the constants in Eqn (7). Here the Dirac delta function only occurs in matrix elements between atomic states. These can be computed to numerical precision in a separate calculation on an isolated atom. This avoids the need to explicitly compute the effect of the delta function on the valence states, and the associated issue of poor numerical convergence.

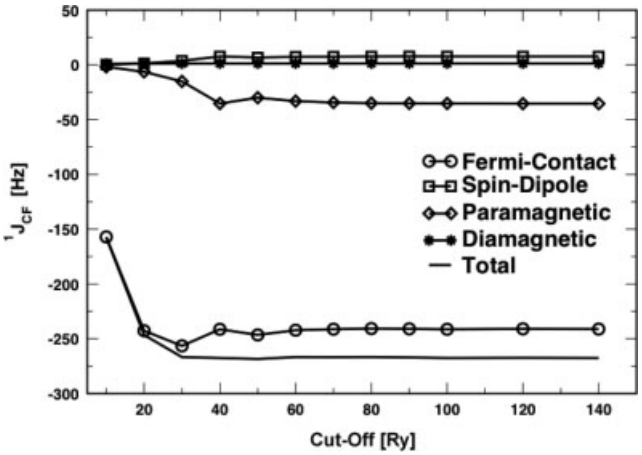

Figure 3. Convergence of the Ramsey components of the $^{19}F-^{13}C$ coupling in CHF_3 with respect to the size of the planewave basis.

Computational cost

A single ***J***-coupling calculation provides ***J*** between one nucleus and all others in the system. In many cases, only a small number of calculations will be required to give all the relevant couplings – either because of symmetry or because the sample has been selectively enriched. In such cases, the calculation of ***J*** is comparable to the cost of computing the magnetic shielding tensors. The most expensive case would be a disordered material, such as a glass, in which we would require a separate calculation for each atom in the system. With the rapid advance of computer technology any benchmark timings quickly become obsolete. Representative timings can be found in Refs [8–10]. To give an indication of the cost, using the most recent generation of processors a calculation on an amino acid with 200 atoms took 22 min to compute the electronic ground-state and a further 72 min to obtain the ***J*** tensor between one nucleus and all others in the system (50 min for the spin terms and 22 min for the orbital contributions). The calculations were run on four dual-quad core Intel Xeon E5540 2.53 GHz processors (ie 32 cores in total). The cost of the calculation scales as the cube of the number of atoms in the system – for this reason calculations on systems with ≈700 atoms are at the limit of present supercomputers.

Experimental Considerations

We now comment on several points which may be important when relating calculated values of ***J*** to NMR experiments.

Reduced coupling constant

As shown in Eqn (2) the observed ***J***-coupling includes a parametric dependence on the gyromagnetic ratios of the nuclear spins. It can be useful to introduce the reduced coupling constant ***K***,

$$\mathbf{K}_{\mathrm{KL}} = \frac{2\pi}{\hbar\gamma_\mathrm{K}\gamma_\mathrm{L}}\boldsymbol{J}_{\mathrm{KL}} \qquad (15)$$

Physically ***K*** corresponds to the coupling between two magnetic moments of unit strength placed at the atomic positions. ***K*** is thus purely a property of the electronic structure of the material. While it might appear unnecessary to have introduced a second (and

not directly measurable) quantity it is worth remembering that it is ***K*** which is obtained from an electronic structure calculation. To see a consequence of this, consider the following example: We have material in which a ***J*** coupling exists between a carbon and a lithium atom; one sample consists of ^{6}Li, the other ^{7}Li. If the measured ***J***-coupling in the ^{6}Li sample is 10 Hz, $\boldsymbol{J} = 26$ Hz will be measured in the ^{7}Li sample. The difference arises completely from the change in γ_{Li} between ^{6}Li and ^{7}Li, and tells us nothing about the electronic structure or bonding in the two materials. As ***K*** is independent of γ_{Li} it is identical for these two samples (neglecting any isotope effects on the bonding). Let us say that for the calculated ^{13}C–^{6}Li coupling we find a 1 Hz difference with respect to experiment. Then for ^{13}C–^{7}Li the error would be 2.6 Hz. Again the difference between the two values arises from the different γ_{Li}. It would not be correct to say that the coupling to ^{6}Li was more computed more accurately than the ^{7}Li coupling.

In a similar vein, care must be taken in comparing ***J*** involving different species. For example, ^{31}P–^{17}O couplings are typically larger than ^{29}Si–^{17}O couplings.[11] Part of this difference is due to the fact that $\gamma_P \approx 2\gamma_{Si}$, and it would be reasonable to expect that calculated errors in ***J*** for ^{31}P-^{17}O couplings would be twice as large as for ^{29}Si–^{17}O couplings.

Decomposition of *J*

Following Eqn (11) the total ***J***-coupling tensor can be divided into several contributions, in particular the isotropic ***J*** has four contributions corresponding to the four mechanisms given in Eqns (5)–(8). Experimentally only the total tensor can be measured, however, the contributions (sometime called the Ramsey terms) can be useful in interpreting the observed ***J***. Quantum chemical studies have shown that several general observations can be made,[25] and so far these have been found to also apply to solid-state systems:[8–11] the DSO term is generally very small; the SD term is usually small, but can play a significant role certain couplings – e.g. those involving ^{19}F; for one bond couplings the PSO and FC terms are dominant; and for longer range couplings usually the FC is the dominant mechanism.

The isotropic ***J*** may take a positive or negative value – trivially this can arise as γ is a signed quantity, but the reduced coupling constant can also take either sign. For example, in Ref. [11] the sign of the computed $^{2}\boldsymbol{J}_{POP}$ varied between SiP_2O_7 polymorphs. Experiments based on spin-echo modulation record only the magnitude of ***J***. The sign of ***J*** has been measured in the solid-state, for example in Ref. [26] $^{2}\boldsymbol{J}_{POP}$ in $Na_4P_2O_4{\cdot}10H_2O$ was observed to be negative. Finally we note that the PSO and FC terms may be of opposite sign and hence in certain cases can cancel leading to very small couplings for directly bonded nuclei. An example of this cancellation is $^{1}\boldsymbol{J}_{CN}$ in pyridine.[27]

Anisotropy of *J* tensors

Experimental and computation studies of the anisotropic components of the ***J***-coupling tensors have been reviewed by Vaara *et al*.[13] Most work has focused on rather symmetric molecules. *Ab-initio* calculations including planewave/PAW calculations on solids, provide the full ***J*** tensor. Calculated principal components for ***J*** tensors involving P, O and Si were reported in Bonhomme *et al*.[11] In Fig.4, we show the orientation of $^{1}\boldsymbol{J}_{PO}$ in an ortep style plot. The tensor is close to axial symmetry with the symmetry axis orientated along the internuclear vector. In this case, the principal components of ***J*** are closely aligned to those of the direct dipolar tensor. However, this symmetry is not enforced (see Ref. [28] for a discussion of the experimental implications of the non-coincidence of ***J*** and D) and further work is required to explore the relation between the orientation of ***J*** and D.

$\boldsymbol{J}_{KL}$ *versus* $\boldsymbol{J}_{LK}$

The symmetric part of ***J*** is unaffected when we interchange the perturbing and receiving nuclei, i.e. $\boldsymbol{J}_{KL} = \boldsymbol{J}_{LK}$. (The antisymmetric part undergoes a sign change under the same conditions – i.e. $\boldsymbol{J}_{KL} = -\boldsymbol{J}_{LK}$[29] see also Ref. [30].) However, $\boldsymbol{J}_{KL}$ and $\boldsymbol{J}_{LK}$ correspond to different calculations: the former considers the spin (or current) induced by the magnetic moment at site L, the latter by the magnetic moment at site K. In each case the induced spin (or current) has a different spacial form – and any numerical imprecision will result in an asymmetry between the two couplings. This means that a comparison of $\boldsymbol{J}_{KL}$ and $\boldsymbol{J}_{LK}$ provides a tough test of the numerical fidelity of the calculations. In practise, in the planewave/PAW scheme, we have found these difference to be small fraction of the coupling (e.g. $\approx$0.1–0.3 Hz for $^{2}\boldsymbol{J}_{POP}$ and $^{2}\boldsymbol{J}_{SiOP}$).

It should be noted that the ability to compute $\boldsymbol{J}_{KL}$ by two different routes mirrors the situation when ***J*** is measured by observing the modulation of spin-echo intensity. For example, in Ref. [10], the one bond ***J*** coupling between C and O in Uracil was obtained twice, first by observation of the spin-echo intensity on ^{13}C and in a subsequent experiment by observation on ^{17}O.

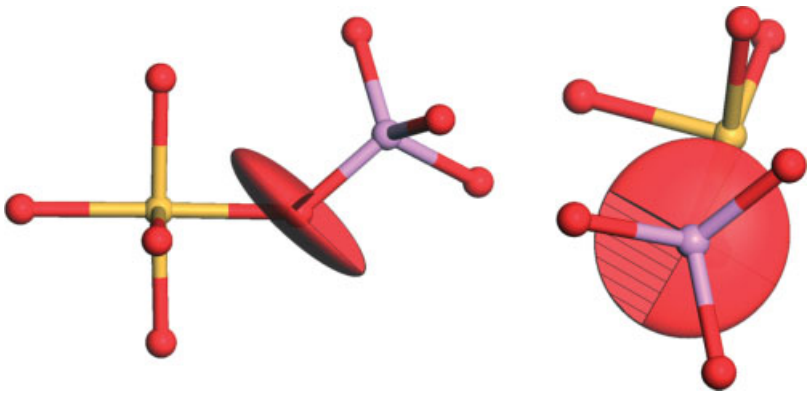

Figure 4. Ellipsoid representation of the symmetric part of a $^{1}\boldsymbol{J}_{PO}$ tensor in the monclinic (AIII) polymorph of SiP_2O_7[11] O, Si, P atoms are shown in red, yellow and purple, respectively.

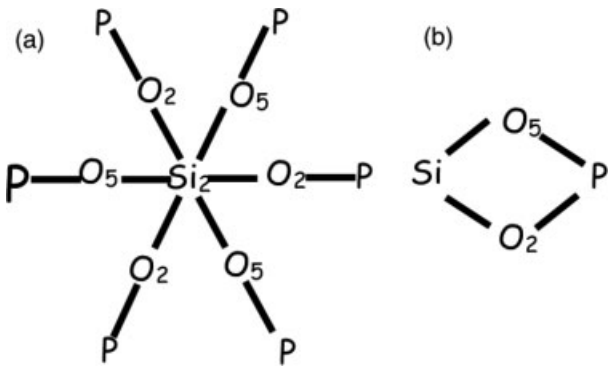

Figure 5. (a) Local environment of the Si2 site in $Si_5O(PO)_4$; (b) hypothetical ring structure in a silicophosphate.

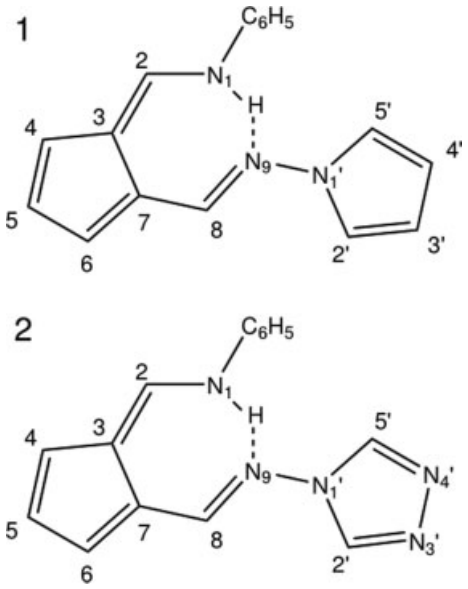

Figure 6. Pyrole (1) and triazole (2) 6-aminofulvene-1-aldimine derivatives.

J and crystal structure

As noted above the ***J***-coupling mechanism breaks the translational symmetry of the crystal. For this reason we must carefully examine the crystal structure to determine the number of unique ***J***-couplings expected for a given system.

Let us consider a physical example. In Fig.5, we show a schematic diagram of the local atomic arrangement around the Si2 site in $Si_5O(PO_4)_6$. Si has six oxygen nearest neighbours, split between two sets of chemically equivalent atoms (3 O2 and 3 O5). The second nearest neighbours are phosphorus – and all six atoms are chemically equivalent under the symmetry operations of the crystal. This chemical equivalence is highlighted by the corresponding chemical shifts: for ^{17}O we would expect two peaks corresponding to O2 and O5 – while for ^{31}P a single peak would be seen. But what about the ***J***-couplings for this system? Clearly there will be two $^1\boldsymbol{J}_{SiO}$ couplings arising from Si2–O2 and Si2–O5. However, there will also be two $^2\boldsymbol{J}_{SiP}$ couplings, both involving Si2 and P. If one makes a link between ***J***-coupling and bonding one coupling arises from the Si–O2–P pathway, the other from Si–O5–P. In other words the P sites are not magnetically equivalent.

A physical interpretation for this magnetic inequivalence is as follows: In the ground-state, all P sites are related by symmetry. However, a magnetic moment placed at the Si2 site will lower the symmetry of the system – and now the P atom bonded to O2 will not be in the same environment as the P atom bonded to O5, i.e. considering the Fermi-contact mechanism the spin density induced at P(O2) will be different to that at P(O5). Experimentally it was found that indeed two unique couplings were needed to fit the spin-echo modulation at Si2[2] – and the values were in good agreement with those computed.[8]

For illustrative purposes, we consider the hypothetical structure shown in Fig. 5 in which Si is bonded to the same P via two distinct oxygen sites. In this case, only a single $^2\boldsymbol{J}_{SiP}$ coupling exists. In making a connection to bonds we would have to say that this coupling corresponds to the sum of the Si–O2–P and Si–O5–P pathways but it would not be experimentally possible to distinguish the contributions. Computationally one could examine the induced spin or current, and make a partition between the pathways but such a division would be arbitrary.

Applications

We now briefly review applications of the planewave pseudopotential approach to the calculation of ***J*** in solid materials. It should be noted that there has been recent work using quantum chemical approaches and cluster models to compute ***J*** in inorganic materials including $^2\boldsymbol{J}_{POP}$ in $(MoO_2)_2P_2O_7$,[31] $^2\boldsymbol{J}_{SiOSi}$ in a calcium silicate[4] and in a silicate zeolite.[32]

Molecular crystals

While results for isolated molecules were provided as part of the initial validation of the planewave/PAW approach in Ref. [8], the first application to crystalline materials was the examination of hydrogen bond mediated ***J*** couplings.[9] Computed and experimental $^2\boldsymbol{J}_{NN}$ couplings are reported in Table 1 for two amino-fulvene derivatives.

These compounds have an intramolecular hydrogen bond – but no hydrogen bonds between molecules, making them an ideal case for the study of solid-state effects on ***J***-coupling. Calculations were performed on three models: the crystalline solid (crys), an isolated molecule taken directly from the crystal (cons. mol.) and an isolated molecule whose geometry had been optimised in vacuum (rel. mol.). The difference between (crys) and (cons. mol.) must be due to electrostatic effects of the crystal lattice. It was found that each coupling increased by ≈0.5 Hz on moving from the solid to crystal (note that as $|\boldsymbol{J}|$ is measured and the couplings are of opposite sign this means that the observed $|^{2h}\boldsymbol{J}_{NN}|$ would increase while $|^2\boldsymbol{J}_{NN}|$ would decrease). The difference between (cons. mol.) and (rel. mol.) is ascribed to changes in the geometry caused by the crystal lattice. This was found to be a small effect for $^2\boldsymbol{J}_{NN}$ but on moving from the (rel. mol.) to the (cons. mol.) model $^{2h}\boldsymbol{J}_{NN}$ decreased by 1.2 Hz reflecting the weaker (longer) hydrogen bond in the crystalline geometry.

Joyce *et al*. also reported $^2\boldsymbol{J}_{NN}$ for a ribbon-like structure of a deoxy-guanosine derivative. Taking into account the two equivalent molecules in the unit cell there are 12 possible $^2\boldsymbol{J}_{NN}$ couplings, two are between molecules across a hydrogen bond, and the others are intramolecular. The results are summarised in Table 2. The largest couplings are $^{2h}\boldsymbol{J}_{N1-N9}$ and there is good agreement between the calculated and measured values. For

Table 1. NMR *J*-coupling for a pyrole and triazole 6-Aminofulvene-1-aldimine

	Pyrole		Triazole	
	$^{2h}J_{N_9-N_1}$	$^{1}J_{N_9-N'_1}$	$^{2h}J_{N_9-N_1}$	$^{1}J_{N_9-N'_1}$
Rel. mol.	9.8	−9.4	9.5	−10.8
Cons. mol.	8.6	−9.4	8.0	−10.7
Solid	8.1	−9.8	7.4	−11.4
Expt (|*J*|)	8.0 ± 0.3	10.2 ± 0.4	7.2 ± 0.1	12.0 ± 0.1

Calculations taken from Joyce *et al.* [9] and experimental values from Brown *et al.* [33] Numbering from Fig. 6.

Table 2. NMR *J*-coupling for a deoxyguanoise derivative

Coupling	Calc (Hz)	Expt (Hz)
$^{2}J_{N_{1a}-N_{2a}}$	2.4	DQ intensity
$^{2}J_{N_{1b}-N_{2b}}$	2.3	DQ intensity
$^{2}J_{N_{1a}-N_{3a}}$	−1.1	–
$^{2}J_{N_{1b}-N_{3b}}$	−1.1	–
$^{2h}J_{N_{1a}-N_{7b}}$	6.5	6.2 ± 0.4
$^{2h}J_{N_{1b}-N_{7a}}$	7.7	7.4 ± 0.4
$^{2}J_{N_{2a}-N_{3a}}$	5.4	6.6 ± 0.7[a]
$^{2}J_{N_{2b}-N_{3b}}$	5.7	
$^{2}J_{N_{3a}-N_{9a}}$	4.4	4.3 ± 0.2[a]
$^{2}J_{N_{3b}-N_{9b}}$	4.2	
$^{2}J_{N_{7a}-N_{9a}}$	−1.2	–
$^{2}J_{N_{7a}-N_{9b}}$	−1.3	–

Calculations taken from Joyce *et al.* [9] and experimental values from Pham *et al.* [34] Numbering taken from Fig. 7 DQ refers to correlations observed in a ^{15}N refocused INADEQUATE spectrum.[35]
[a] average value observed.

remaining couplings only the four between N2/N3 and N3/N9 could be measured,[34] and the calculations show that these indeed correspond to the largest of the intramolecular couplings. The couplings next in size are between N1/N2 and while values of *J* could not be extracted experimentally, DQ correlations were present between N1 and N2 in a ^{15}N refocused INADEQUATE spectrum.[35] At about 1 Hz the couplings between N1/N3 and N7/N9 have the smallest computed *J*.

In Ref. [10], calculations of *J* involving ^{13}C, ^{15}N, ^{17}O were presented for crystalline forms of uracil and glycine·HCl. Comparison was made to MAS-spin-echo measurements. The computed and experimental results are summarised in Table 3. For these challenging experiments, the calculations played an important role in determining both the feasibility and interpretation of the experiments. One aspect of this is that the calculations identify all of the relevant couplings to a given a nucleus. For example, to interpret the hetronuclear ^{17}O/^{13}C spin-echo measurements in glycine·HCl it was necessary to take into account $^{2}J_{OO}$ as well as $^{1}J_{OC}$. Similarly, for interpretation of the hetronuclear ^{15}N/^{17}O spin-echo measurements in Uracil in was necessary to include the intramolecular $^{2}J_{NN}$ as well as the intramolecular $^{2h}J_{NO}$. In Uracil, there are two coupling pathways between sites N3 and O4. The calculation provide values for both, and it can be seen that the two bond intramolecular coupling is much smaller than the two bond coupling across the O–HN hydrogen bond.

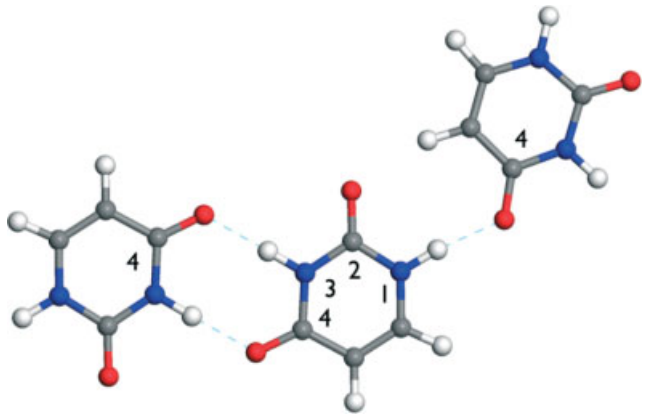

Figure 8. Crystal structure of uracil. Nitrogen, oxygen, carbon, and hydrogen atoms are represented as blue, red, grey, and white circles, respectively.

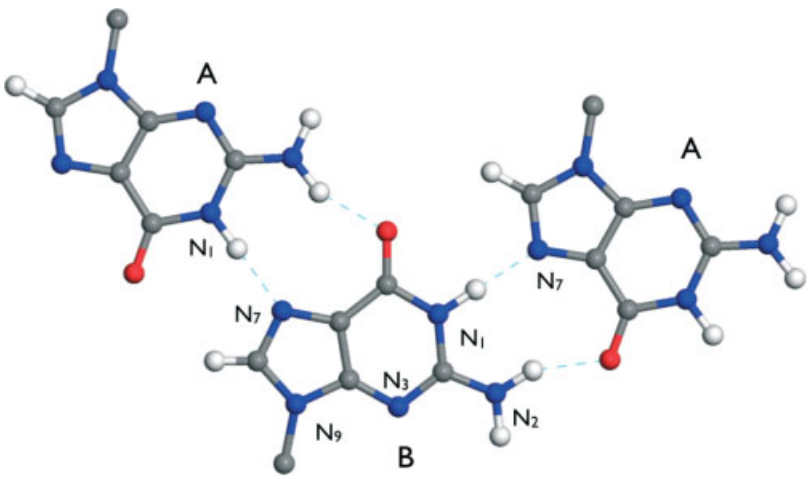

Figure 7. Crystal structure of the short-chained deoxyguanosine[36] showing the two inequivalent molecules (labelled A and B). Nitrogen, oxygen, carbon, and hydrogen atoms are represented as blue, red, grey, and white circles, respectively.

Table 3. Calculated NMR chemical shifts and *J*-coupling for Uracil and Glycine·HCl

Coupling	Calc	Expt	
Uracil			
$^{2}J_{N_1-N_3}$	2.7	2.7 ± 0.1	
$^{2}J_{N_3-O_4}$	0.5		
$^{2h}J_{N_3-O_4}$	4.6	4.8 ± 0.5[a]	5.1 ± 0.6[b]
$^{2h}J_{N_1-O_4}$	6.1	6.7 ± 0.4[a]	
Glycine·HCl			
$^{1}J_{C-O_1}$	27.5	25.3 ± 0.3[c]	26.7 ± 0.6[d]
$^{1}J_{C-O_2}$	24.9	24.7 ± 0.2[c]	
$^{2}J_{O_1-O_2}$	7.9	8.8 ± 0.9	

Taken from Hung *et al.* [10] Numbering taken from Figs 8 and 9. [a] from observations on ^{15}N [b] average value from observations on ^{17}O, [c] from observations on ^{17}O, [d] average value from observations on ^{13}C.

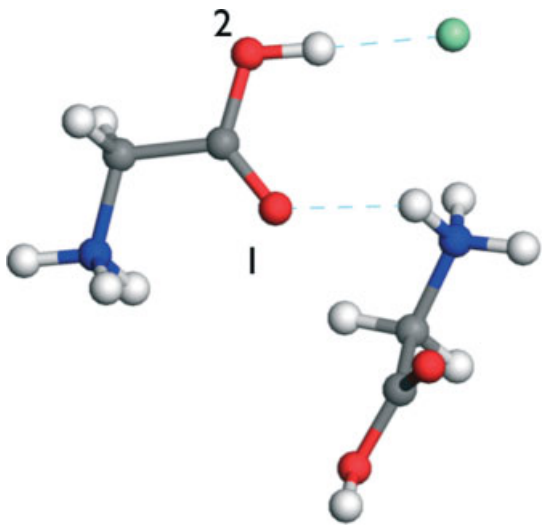

Figure 9. Crystal structure of glycine·HCl. Nitrogen, oxygen, carbon, and hydrogen atoms are represented as blue, red, grey, and white circles, respectively.

Inorganic materials

Calculations of $^{2}J_{SiOP}$ were reported for $Si_5O(PO_4)_6$ in Ref. [8] and compared against experimental results from Coelho *et al.*[2] As shown in Table 4 the calculated couplings range from 17 to 1 Hz, and are in good agreement with experiment. The presence of two unique couplings between the Si2 and P sites was discussed above. Calculated $^{2}J_{SiOP}$ have been reported for three polymorphs of SiP_2O_7 in Ref. [11]. For the two monoclinic forms (AIII and AIV) of SiP_2O_7 the silicon site is coordinated by six different oxygens which complicates the analysis of the spin-echo modulations. However, the experimental modulation was found to give good agreement when compared to the average of the computed couplings. Calculated $^{1}J_{SiO}$ and $^{1}J_{PO}$ were also reported for these compounds. As might be expected $^{1}J_{PO}$ are generally larger than $^{1}J_{SiO}$. For each of the calculated couplings the principal components and anisotropy of *J* was reported – in all cases the anisotropy was significant.

Table 4. Calculated NMR chemical shifts and *J*-coupling for silicophosphate $Si_5O(PO_4)_6$

Coupling	^{31}P [ppm]	^{29}Si [ppm]	Calc. [Hz]
$J^2_{P-O_3-Si_1}$	−47.4 (−43.8)	−214.8 (−213.3)	−17.12 (15 ± 2)
$J^2_{P-O_2-Si_2}$		−218.7 (−217.0)	−16.26 (14 ± 2)
$J^2_{P-O_5-Si_2}$		−218.7 (−217.0)	−1.17 (4 ± 2)
$J^2_{P-O_4-Si_3}$		−128.6 (−119.1)	−14.13 (12 ± 2)

The experimental values[2] are in brackets. Taken from Ref. [8].

Outlook

Initial calculations of NMR *J*-couplings for solid materials using the planewave pseudopotential formalism have demonstrated the accuracy and utility of the approach. From a computational point of view, two developments would extend the range of systems to which the present approach could be applied. Firstly, the current implementation uses norm-conserving pseudopotentials. An extension to the more computationally efficient ultrasoft potentials[37] (as has been done for magnetic shielding[38]) would allow semi-core states to be included in the calculations. This would enable efficient calculation of *J* involving transition metals. The second area involves including relativistic effects to compute couplings involving heavy elements. Quantum chemical calculations have shown these can be significant for *J*.[39] A significant fraction of the relativistic effects on magnetic shieldings cancel out when comparing to experimental chemical shifts. However, *J*-coupling is an absolute quantity and no such cancellation occurs. Immediate applications would include couplings between ^{207}Pb and ^{19}F.[40]

Acknowledgements

J.R.Y. would like to thank Siân Joyce for her central contribution to the development of theory and software to compute *J* tensors in solids. He is grateful to Christian Bonhomme (Paris) and Steven Brown (Warwick) for numerous useful discussions. Funding was provided by the Royal Society (UK) and computer resources by the Oxford Supercomputing Centre.

References

[1] D. Massiot, F. Fayon, M. Deschamps, S. Cadars, P. Florian, V. Montouillout, N. Pellerin, J. Hiet, A. Rakhmatullin, C. Bessada, *Compt. Rend. Chim.* **2010**, *13*, 117.
[2] C. Coelho, T. Azaïs, L. Bonhomme-Coury, G. Laurent, C. Bonhomme, *Inorg. Chem.* **2007**, *46*, 1379.
[3] P. Guerry, M. E. Smith, S. P. Brown, *J. Am. Chem. Soc.* **2009**, *131*, 11861.
[4] P. Florian, F. Fayon, D. Massiot, *J. Phys. Chem. C* **2009**, *113*, 2562.
[5] P. Blaha, K. Schwarz, P. Sorantin, S. Trickey, *Comput. Phys. Commun.* **1990**, *59*, 399.
[6] P. Blaha, P. Sorantin, C. Ambrosch, K. Schwarz, *Hyperfine Interact.* **1989**, *51*, 917.
[7] C. J. Pickard, F. Mauri, *Phys. Rev. B* **2001**, *63*, 245101.
[8] S. A. Joyce, J. R. Yates, C. J. Pickard, F. Mauri, *J. Chem. Phys.* **2007**, *127*, 204107.
[9] S. A. Joyce, J. R. Yates, C. J. Pickard, S. P. Brown, *J. Am. Chem. Soc.* **2008**, *130*, 12663.
[10] I. Hung, A.-C. Uldry, J. Becker-Baldus, A. Webber, A. Wong, M. E. Smith, S. A. Joyce, J. R. Yates, C. J. Pickard, R. Dupree, S. P. Brown, *J. Am. Chem. Soc.* **2009**, *131*, 1820.

[11] C. Bonhomme, C. Gervais, C. Coelho, F. Pourpoint, T. Azaïs, L. Bonhomme-Coury, F. Babonneau, G. Jacob, M. Ferrari, D. Canet, J. R. Yates, C. J. Pickard, S. A. Joyce, F. Mauri, D. Massiot, *Magn. Reson. Chem.* **2010**, (in press). DOI 10.1002/mrc.2635.
[12] T. Helgaker, M. Jaszunski, K. Ruud, *Chem. Rev.* **1999**, *99*, 397.
[13] J. Vaara, J. Jokisaari, R. E. Wasylishen, D. L. Bryce, *Prog. Nucl. Magn. Reson. Spectrosc.* **2002**, *41*, 233.
[14] T. Helgaker, M. Jaszunski, M. Pecul, *Prog. Nucl. Magn. Reson. Spectrosc.* **2008**, *53*, 249.
[15] R. K. Harris, P. Hodgkinson, C. J. Pickard, J. R. Yates, V. Zorin, *Magn. Reson. Chem.* **2007**, *45*, S174.
[16] J. R. Yates, C. J. Pickard, Computations of magnetic resonance parameters for crystalline systems: principles, *Encyclopedia of Magnetic Resonance*, (Eds: R. K. Harris, R. Wasylishen), John Wiley: Chichester, UK, **2008**.
[17] M. C. Payne, M. P. Teter, D. C. Allen, T. A. Arias, J. D. Joannopoulos, *Rev. Mod. Phys.* **1992**, *64*, 1045.
[18] R. M. Martin, *Electronic Structure: Basic Theory and Practical Methods*, Cambridge University Press: UK, **2004**.
[19] N. F. Ramsey, E. M. Purcell, *Phys. Rev.* **1952**, *85*, 143.
[20] N. F. Ramsey, *Phys. Rev.* **1953**, *91*, 303.
[21] S. Baroni, S. de Gironcoli, A. Dal Corso, P. Giannozzi, *Rev. Mod. Phys.* **2001**, *73*, 515.
[22] V. Milman, K. Refson, S. J. Clark, C. J. Pickard, J. R. Yates, S.-P. Gao, P. J. Hasnip, M. I. J. Probert, A. Perlov, M. D. Segall, *J. Mol. Struct. THEOCHEM* **2010**, DOI: 10.1016/j.theochem.2009.12.040.
[23] C. G. van de Walle, P. E. Blöchl, *Phys. Rev. B* **1993**, *47*, 4244.
[24] F. Jensen, *J. Chem. Theory Comput.* **2006**, *2*, 1360.
[25] N. H. Contreras, V. Barone, J. C. Facelli, J. E. Peralta, *Advances in Theoretical and Physical Aspects of Spin-Spin Coupling Constants*, vol. 51, (Ed: G. Webb), Academic Press: **2003**.
[26] S. Dusold, W. Milius, A. Sebald, *J. Magn. Reson.* **1998**, *135*, 500.
[27] J. E. Del Bene, J. Elguero, *Magn. Reson. Chem.* **2006**, *44*, 784.
[28] D. L. Bryce, N. M. D. Courchesne, F. A. Perras, *Solid State Nucl. Magn. Reson.* **2009**, *36*, 182.
[29] A. D. Buckingham, P. Pyykkö, J. B. Robert, L. Wiesenfeld, *Mol. Phys.* **1982**, *46*, 177.
[30] K. J. Harris, D. L. Bryce, R. E. Wasylishen, *Can. J. Chem.* **2009**, *87*, 1338.
[31] S. E. Lister, A. Soleilhavoup, R. L. Withers, P. Hodgkinson, J. S. O. Evans, *Inorg. Chem.* **2010**, *49*, 2290.
[32] S. Cadars, D. Brouwer, B. Chmelka, *Phys. Chem. Chem. Phys.* **2009**, *11*, 1825.
[33] S.P. Brown, M. Perez-Torralba, D. Sanz, R.M. Claramunt, L. Emsley, *Chem. Commun.* **2002**, 1852.
[34] T. N. Pham, J. M. Griffin, S. Masiero, S. Lena, G. Gottarelli, P. Hodgkinson, C. Filip, S. P. Brown, *Phys. Chem. Chem. Phys.* **2007**, *9*, 3416.
[35] T. N. Pham, S. Masiero, G. Gottarelli, S. P. Brown, *J. Am. Chem. Soc.* **2005**, *127*, 16018.
[36] T. Giorgi, I. Grepioni, I. Manet, S. Mariani, S. Masiero, E. Mezzina, S. Pieraccini, L. Saturni, G. Spada, G. Gottarelli, *Chem.–Eur. J.* **2002**, *8*, 2143.
[37] D. Vanderbilt, *Phys. Rev. B* **1990**, *41*, 7892.
[38] J. R. Yates, C. J. Pickard, F. Mauri, *Phys. Rev. B* **2007**, *76*, 024401.
[39] J. Autschbach, T. Ziegler, *J. Chem. Phys.* **2000**, *113*, 936.
[40] C. Martineau, F. Fayon, C. J.-P. Legein, G. S. Buzaré, D. Massiot, *Chem. Commun.* **2007**, 2720.

